Available online at www.sciencedirect.com
SCIENCE DIRECT®
Icarus 180 (2006) 1–7
ICARUS
www.elsevier.com/locate/icarus

Regolith properties in the south polar region of the Moon from 70-cm radar polarimetry

Bruce A. Campbell [a,*], Donald B. Campbell [b]

[a] *Center for Earth and Planetary Studies, Smithsonian Institution, MRC 315, Washington, DC 20560-0315, USA*
[b] *Cornell University, Space Sciences Building, Ithaca, NY 14853-6801, USA*

Received 18 October 2004; revised 25 July 2005

Available online 10 November 2005

Abstract

The south polar region of the Moon contains areas permanently shadowed from solar illumination, which may provide cold traps for volatiles such as water ice. Previous radar studies have emphasized the search for diagnostic polarization signatures of thick ice in areas close to the pole, but near-surface regolith properties and regional geology are also important to upcoming orbital studies of the shadowed terrain. To study regional regolith variations, we collected 70-cm wavelength, 450-m resolution, dual-circular polarization radar data for latitudes 60–90° S using the Arecibo and Greenbank telescopes. The circular polarization ratio, μ_c, is sensitive to differences in rock abundance at the surface and up to tens of m below the surface, depending upon the regolith loss tangent. We observe significant variations in μ_c, attributed to changes in the surface and subsurface rock population, across the south polar highlands. Concentric haloes of low polarization ratio surrounding Hausen, Moretus, and other young craters represent rock-poor ejecta layers. Values of μ_c up to ~1 occur in the floors and near-rim deposits of Eratosthenian and Copernican craters, consistent with abundant rocky ejecta and/or fractured impact melt. Enhanced μ_c values also correspond to areas mapped as Orientale-derived, plains-forming material [Wilhelms, D.E., Howard, K.A., Wilshire, H.G., 1979. USGS Map I-1162], and similar polarization properties characterize the permanently shadowed floors of craters Faustini and Shoemaker. Small areas of very high (>1.5) circular polarization ratio occur on shadowed and seasonally sunlit terrain, and appear to be associated with small craters. We suggest that regolith in low-lying areas near the south pole is characterized by a significant impact melt component from Orientale, which provides a source for excavation of the block-rich ejecta around small craters observed in this and earlier radar studies. The lower portion of the interior wall of Shackleton crater, permanently shadowed from the sun but visible from Earth, is not significantly different in 70-cm scattering properties from diurnally/seasonally sunlit areas of craters with similar morphology.

Keywords: Moon; Radar; Regoliths

1. Introduction

The lunar polar regions contain areas that are permanently shadowed from solar illumination (Margot et al., 1999; Bussey et al., 1999), which may provide "cold traps" for volatiles delivered by comets or formed by solar wind interactions with the regolith (e.g., Crider and Vondrak, 2000). Imaging radar, either from the Earth during favorable librations or from an orbital sensor, is the only method likely to yield high-resolution (<1 km) images of these shadowed areas. Radar also offers the opportunity to probe the regolith to depths of meters to tens of meters, depending upon the radar wavelength and the regolith loss tangent.

Previous radar studies of the south pole have emphasized a search for cold trap locations based on interferometric topographic maps (Margot et al., 1999), and for the diagnostic backscatter and polarization signature of thick ice deposits (Stacy et al., 1997). These studies used radar wavelengths of 3–12.6 cm, and typically imaged areas at latitudes >80° S with spatial resolutions of 75–125 m. Radar observations at 70-cm wavelength permit mapping of a much larger region in a single observing run (due to the broader antenna beam pattern), albeit at a lower (450 m) spatial resolution. The 70-cm signals also

* Corresponding author. Fax: +1 202 786 2566.
E-mail address: campbellb@si.edu (B.A. Campbell).

0019-1035/$ – see front matter
doi:10.1016/j.icarus.2005.08.018

penetrate to greater depth, increasing our sensitivity to variations in the integrated regolith rock abundance.

The Lunar Prospector (LP) neutron spectrometer identified enhanced hydrogen abundance near both poles, which could be attributed to 1–2% water ice within the upper meter of the regolith in permanently shadowed craters (Feldman et al., 2001). The LP data are of too coarse resolution to determine the degree of localized volatile concentration. Earth-based 12.6-cm radar observations show enhanced backscatter and circular polarization ratio only in association with the walls and proximal ejecta of impact craters or likely craters smaller than can be resolved by the imagery. No contiguous, high-backscatter regions covering crater floors, similar to polar features on Mercury attributed to ice (Butler et al., 1993; Harmon et al., 1994; Black et al., 2002), are evident (Stacy et al., 1997; Campbell et al., 2003). The Clementine spacecraft radio transmitter and an Earth-based receiver were used to acquire bistatic radar echoes from the Moon. These data have been interpreted to indicate a localized concentration of ice on the lower interior wall of Shackleton crater (Nozette et al., 1996; 2001), but their analysis and interpretation are questioned by Simpson and Tyler (1999). In all of these studies, the areas of permanent shadow visible from Earth represent perhaps $1/4$ of the total shadowed terrain.

The search for concentrated ice at the lunar poles thus remains inconclusive. We have strong evidence for some fraction of a hydrogen-bearing phase within the lunar regolith near the poles, but whether this is in the form of water ice confined to permanently shadowed craters, and to what degree such ice is concentrated, remain uncertain. These issues will be addressed, in part, by the thermal radiometer, ultraviolet imager, and neutron spectrometer on the Lunar Reconnaissance Orbiter. The south polar regional geology and the properties of the near-surface regolith in shadowed terrain are of considerable importance to the interpretation of these data. In this paper, we present new dual-polarization, 70-cm wavelength radar images that cover the entire nearside polar region (60–90° S), and 6–7° of the farside, at a spatial resolution of ∼450 m/pixel. We use variations in backscatter strength and the circular polarization ratio to study the near-surface properties of cold trap terrain, and to trace the likely areal extent of Orientale basin ejecta.

2. Radar data

We transmit a left-circular polarized radar signal from the 305-m Arecibo telescope, and receive lunar echoes, in both senses of circular polarization, at the 105-m Greenbank Telescope (GBT) in West Virginia. The complex-valued data, denoted as same-sense (SC or left-circular transmit, left-circular receive) and opposite-sense (OC or left-circular transmit, right-circular receive) are processed using standard delay–Doppler techniques.

The delay–Doppler images are projected to a lunar cartographic framework using ephemeris predictions that describe the range and frequency shift of any given point with respect to the observing station. The delay and Doppler trajectory with time for each pixel is slightly different, with the difference increasing with distance from the center of the target area. To avoid smearing of the radar image, we employ a focusing method that maps the area in small "chunks" after compensating for the time-varying delay and frequency shifts at the center of the chunk. Using a 3 μs pulse and a 990 s look, we obtain a horizontal spatial resolution of ∼450 × 320 m near the pole. The final images represent averages over three separate looks, resampled at 400-m resolution (Fig. 1). The pole is imaged at a radar incidence angle of ∼84°. Contours of constant incidence angle approximately parallel the radar-visible "limb" of the Moon.

The penetration depth of the radar signal is dependent upon the illuminating wavelength, λ, and the loss tangent, $\tan\delta$, of the regolith. To first order, the probing length is given by $\lambda/(2\pi\sqrt{\varepsilon'}\tan\delta)$, where ε' is the real dielectric constant of the regolith. For a radar wavelength of 0.7 m and a real dielectric constant of 2.7 (Carrier et al., 1991), we obtain a probing length, in meters, of $\sim 0.07/\tan\delta$. Near the poles, the high incidence angle means that the refracted wave that penetrates the surface travels at a significant angle to the vertical, so the penetration depth is about 80% of the probing length. The loss tangent of highlands material ranges from 0.01 to 0.001, though some samples have even lower values (Carrier et al., 1991). The 70-cm penetration depth is thus 6–60 m, depending upon regolith dielectric properties.

Measurements in the two polarization states may be used to determine the circular polarization ratio, $\mu_c = \mathrm{SC/OC}$ (Fig. 2). The relative power in the two polarizations is calibrated to the measured noise level in a portion of the data that does not contain echoes from the Moon. We calculate the polarization ratio from SC and OC images that are boxcar-filtered over 5×5 pixel areas. This yields a 75-look average value for each location, an effective spatial resolution of ∼2 km, and an approximate uncertainty of ± 0.12 in μ_c. The polarization ratio is generally higher for targets with greater diffuse scattering due to surface or subsurface rocks. Values greater than unity are associated with coherent backscatter from thick (meter-scale or greater) ice, or from very rugged, blocky terrain (Hapke, 1990; Campbell et al., 1993). Values of μ_c for regolith with modest amounts (a few percent) of ice as small inclusions or thin layers will be little different from those of normal "dry" lunar terrain.

One aspect of our data that differs from previous lunar radar studies is the separation of Arecibo and the GBT, which leads to a bistatic phase angle of ∼0.4° between the transmitter and receiver. This bistatic phase angle will lead to some reduction in the circular polarization ratio for a target characterized by coherent backscatter (e.g., thick ice), but phase angles >1–2° are required to entirely suppress such an effect (e.g., Fig. 1 in Nozette et al., 2001). High circular polarization ratios in areas with numerous surface and near-surface blocks on the scale of the radar wavelength will not be affected.

3. Geology of the south polar region

The new 70-cm radar data provide a synoptic view of the south polar highlands that complements earlier geologic mapping from Lunar Orbiter data (Wilhelms et al., 1979). The

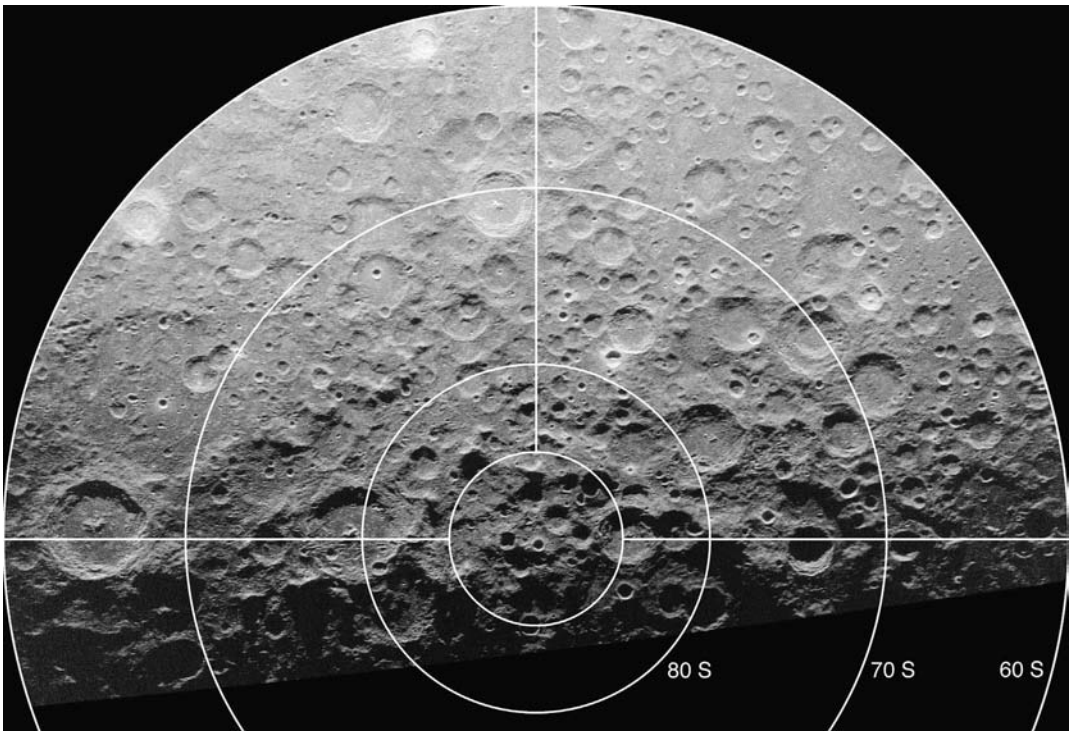

Fig. 1. 70-cm wavelength, opposite-sense circular polarization radar map of the south polar region. Polar stereo projection; zero longitude at top. Latitude parallels marked; interior circle corresponds to 85° S.

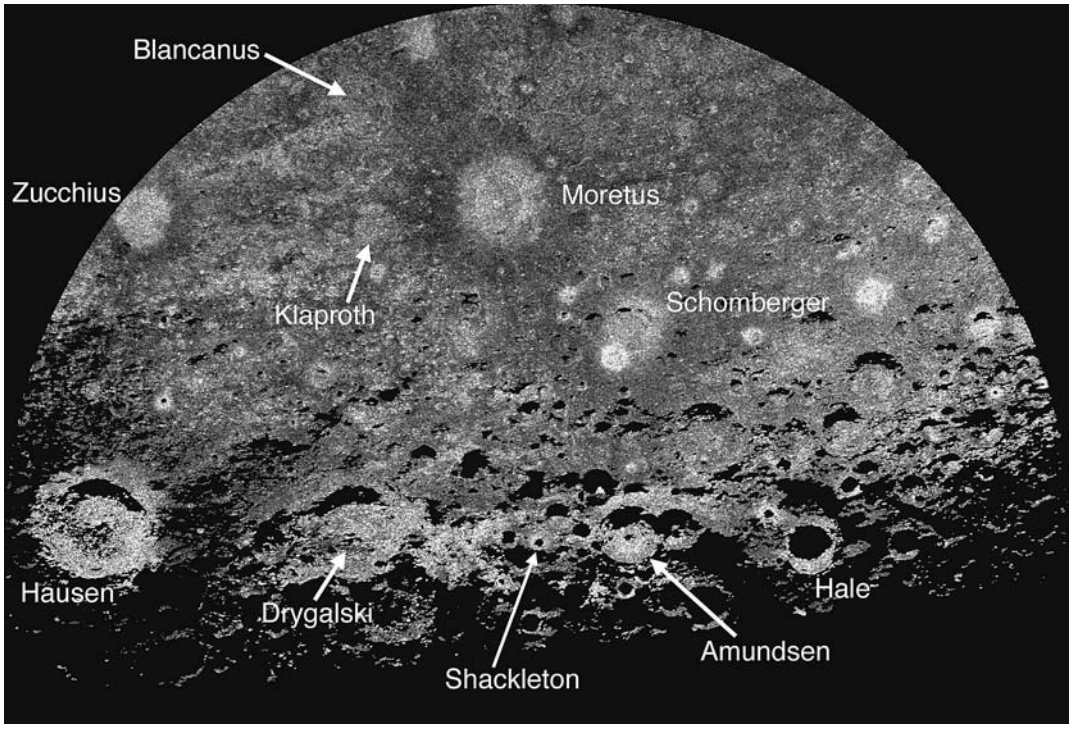

Fig. 2. 70-cm wavelength circular polarization ratio for the region shown in Fig. 1. Areas in radar shadow are set to zero. Image stretch shows polarization ratio from black = 0.5 to white = 1.1. Concentric haloes of low polarization ratio, attributed to rock-poor ejecta, surround Zucchius, Hausen, Moretus, and Schomberger craters.

mega-regolith within this region is comprised of contributions from a number of large basin-forming impacts, including the oldest preserved structure on the Moon, South-Pole Aitken basin (Wilhelms, 1987). Overprinted on the ancient basin structures are ejecta from younger basins and craters. Material ejected from Orientale, the youngest major basin, appears to play a very significant role in the near-surface properties of the area surrounding the pole.

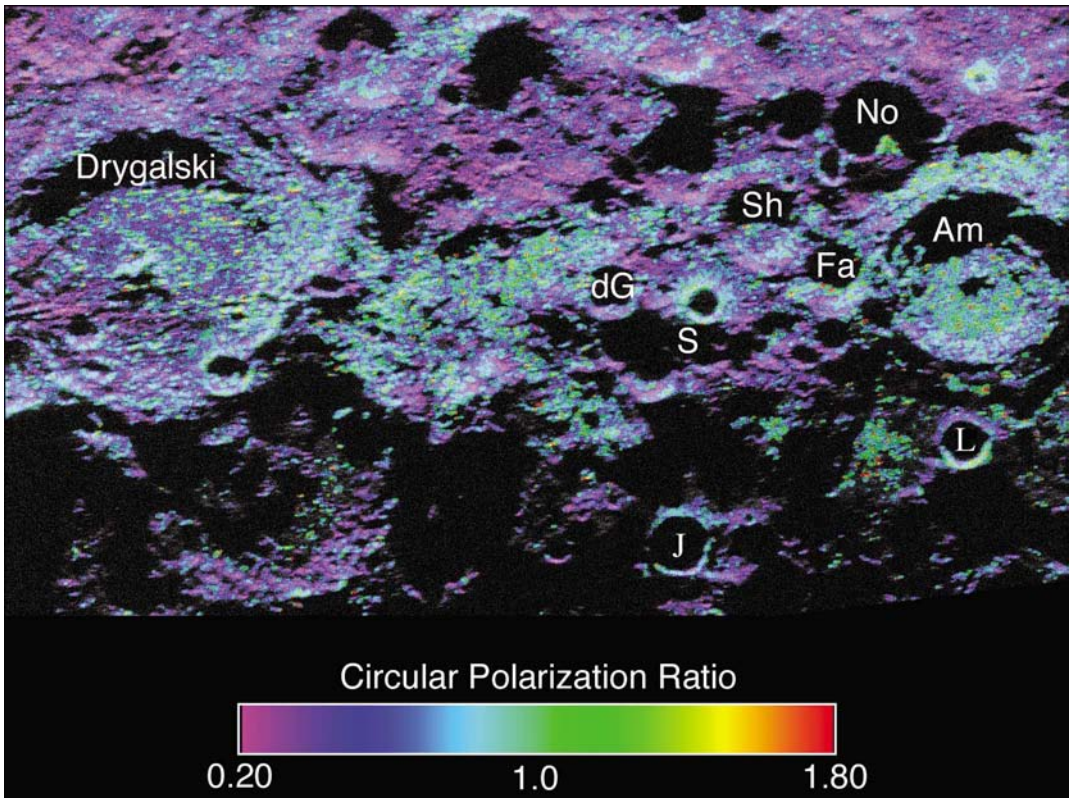

Fig. 3. Color map of circular polarization ratio, μ_c, overlain on OC radar image of area near the south pole. Crater names shown as abbreviations: dG = de Gerlache, Sh = Shoemaker, Fa = Faustini, Am = Amundsen, No = Nobile, S = Shackleton, L = Idelson L, J = Wiechert J.

There are concentric regions of low μ_c values surrounding Zucchius, Hausen, Moretus, and Schomberger craters, consistent with other radar-dark haloes identified by Ghent et al. (2005) (Fig. 2). Possible haloes surround other, smaller Eratosthenian and Copernican craters. The haloes represent areas of relatively rock-poor comminuted ejecta that mantles the "average" highland regolith. The extent of these deposits is considerable, and illustrates how distal crater ejecta contributes to regolith development over time.

Enhanced ($\sim$1) μ_c values are associated with the floors of Hausen, Zucchius, Drygalski, Amundsen, and Hedervari craters, their proximal ejecta, and a patch of highland terrain between Drygalski and de Gerlache craters (Fig. 3). There is also an area of enhanced μ_c in a sunlit portion of Nobile crater. The enhanced polarization ratios associated with the floors and proximal ejecta of Eratosthenian (e.g., Hausen) and Copernican (e.g., Zucchius) craters are readily attributed to impact melt sheets with pervasive meter-scale fracturing, and to abundant comminuted blocks formed by the impact event (e.g., Thompson et al., 1979).

More intriguing are the elevated polarization ratio values associated with some "smooth" crater floors (e.g., Shoemaker and Faustini) and inter-crater highlands (Fig. 3). In general, μ_c enhancements in sunlit areas are correlated with low-relief, Imbrian-period plains material, mapped as "unit Ip" by Wilhelms et al. (1979) and attributed to basin-forming impacts. Such material covers the floors of Amundsen (Fig. 4) and Drygalski (Fig. 5) craters, and enhanced polarization ratios trace similar deposits in Klaproth crater and between Blancanus and Zucchius craters (Fig. 2). We do not observe enhanced μ_c values in Imbrian-period basin-related materials characterized by abundant secondary craters (units Ioc and Ioho of Wilhelms et al., 1979), nor in Nectarian-period lineated and plains-forming deposits (units Nbl and Ntp of Wilhelms et al., 1979). Based on these correlations, we suggest that the floors of craters Shoemaker and Faustini, and local lows in the highlands surrounding the south pole, are likely covered by smooth plains material related to Orientale.

It is interesting that the "smooth plains" material exhibits a higher average polarization ratio than the furrowed and pitted basin ejecta facies. Smooth distal plains related to large basins have been attributed to ponding of impact melt, where furrowed and pitted terrain likely forms through local reworking of the surface by secondary impactors (Eggleton and Schaber, 1972; Moore et al., 1974; Wilhelms, 1987). At such great distances from the basin, the plains-forming units may only be partially comprised of melt rock, but this could still serve to create layers or blocks within the regolith. These would provide subsequent small impacts with a richer source of competent material for fragmentation into decimeter-sized rocks than is available in an older (e.g., pre-Nectarian or Nectarian) highland regolith, leading to an enhanced circular polarization ratio. The same situation is observed in the maria, where younger flows are characterized by a greater surface population of rocks than older flows with deeper regolith cover (Shorthill, 1973). A near-surface melt-rich layer may thus explain the presence of blocky,

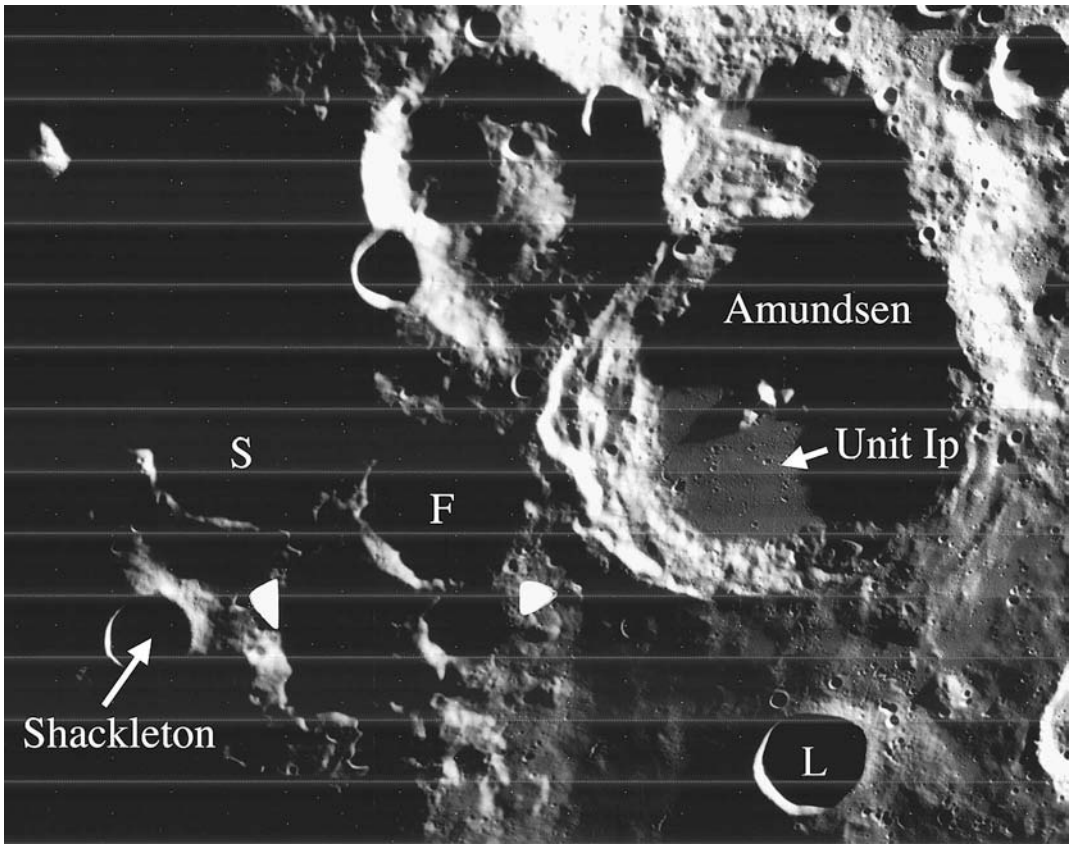

Fig. 4. Portion of Lunar Orbiter Frame IV-094H1, showing the area of the south pole and Amundsen crater. Craters Shoemaker and Faustini are indicated by letters S and F, respectively. L denotes crater Idelson L. Low-relief, Imbrian age plains (unit Ip of Wilhelms et al., 1979) in Amundsen floor, characterized by high circular polarization ratio, marked by arrow. Surrounding pre-Nectarian and Nectarian deposits are not characterized by enhanced circular polarization ratio.

high-μ_c ejecta surrounding small craters in the polar shadowed terrain (Stacy et al., 1997).

4. Observations related to possible ice deposits

On the basis of Clementine bistatic radar data, Nozette et al. (2001) suggest that the lower interior wall of Shackleton crater has some coverage of mixed ice/regolith deposits. The 70-cm radar penetrates to greater depth than the 12.6-cm signals used by earlier Arecibo or Clementine studies, and is expected to reveal any contiguous, meter-scale thicknesses of ice within at least the upper 5 m of the highland regolith. In general, we do not observe contiguous (i.e., 10-km scale), high-μ_c signatures on the floors of craters such as Shoemaker and Faustini. The highest μ_c values, up to ~2, occur in patchy clusters on the floors of both shadowed and sunlit craters (Fig. 3). Based on Lunar Orbiter photos, higher-resolution radar data (Stacy et al., 1997; Margot et al., 1999), and the radar scattering properties of terrestrial rugged terrain (Campbell et al., 1993), we suggest that these patterns reflect the proximal ejecta blankets of abundant small craters.

The circular polarization ratio of crater walls varies considerably with their morphology. Large, older craters with terraced walls (Drygalski, Amundsen) tend to have moderate values of μ_c. Younger craters such as Hausen have very strong polarization ratio enhancements due to a greater population of near-surface rugged blocks. Smaller craters with sharply-defined rims, such as Shackleton, Idelson L, and Wiechert J, have high μ_c values (~1). Craters of similar size with less distinct rims, such as de Gerlache, have little polarization ratio enhancement. Given that high μ_c values occur on both shadowed and diurnally/seasonally sunlit crater walls, we concur with earlier assessments (Stacy et al., 1997) that these variations are likely due to surface morphologic properties rather than to near-surface ice deposits.

5. Conclusions

We present new 70-cm wavelength, dual-circular polarization radar data for the Moon's south polar region (60–90° S), collected using the Arecibo and Greenbank telescopes. We observe significant variations in μ_c, attributed to changes in the surface and subsurface rock population, across the south polar highlands. Concentric haloes of low polarization ratio surrounding Hausen, Moretus, and other young craters represent rock-poor ejecta layers. Values of μ_c up to ~1 occur in the floors and near-rim ejecta of Eratosthenian and Copernican craters, consistent with abundant rocky ejecta and/or fractured impact melt. Enhanced μ_c values also correspond to areas mapped as Orientale-derived, plains-forming material (Wilhelms et al., 1979), and similar polarization properties characterize the permanently shadowed floors of craters Faus-

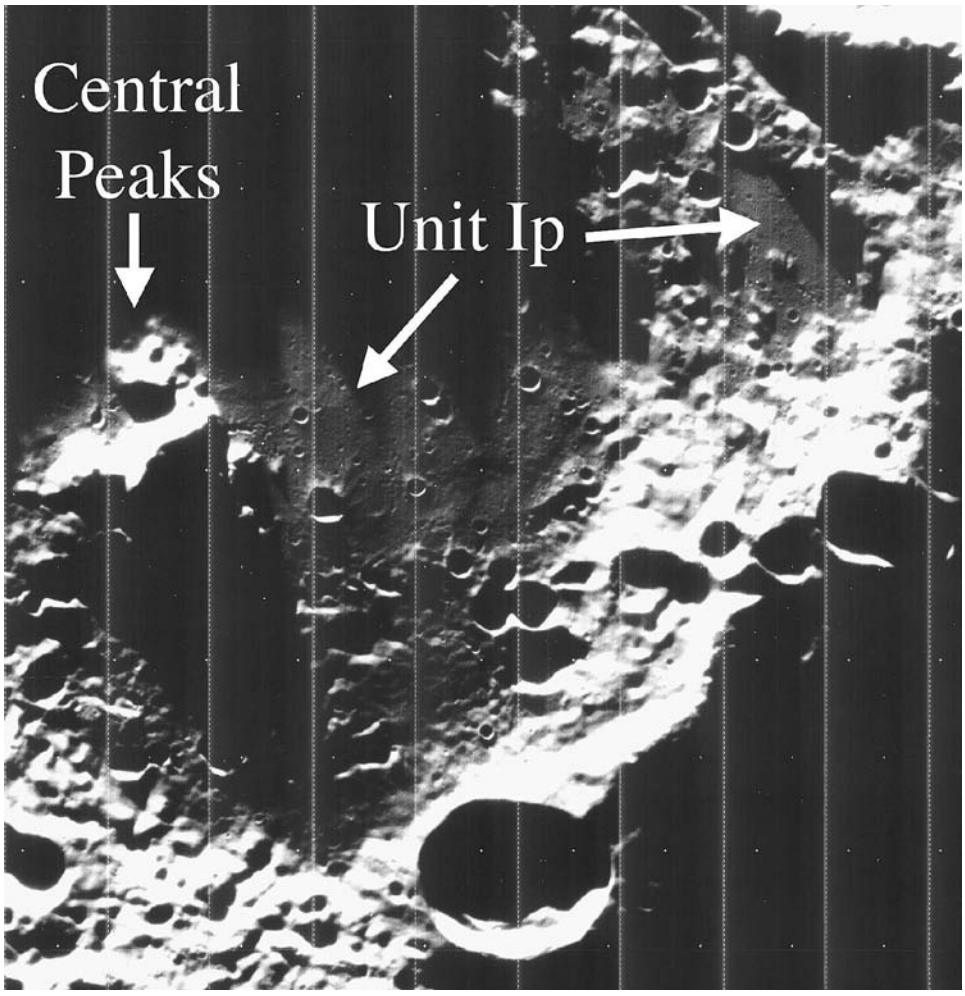

Fig. 5. Portion of Lunar Orbiter Frame IV-193H1, showing the central peaks and eastern floor and rim of Drygalski crater. The arrows mark low-relief Imbrian-age plains units (unit Ip of Wilhelms et al., 1979) that cover the northern crater floor and are perched on the rugged rim topography; both areas are marked by high circular polarization ratio.

tini and Shoemaker. Small areas of very high (>1.5) circular polarization ratio occur on shadowed and sunlit terrain, and appear to be associated with small craters. We suggest that regolith in low-lying areas near the south pole is characterized by a significant impact melt component from Orientale, which may explain the block-rich ejecta around small craters observed in this and earlier radar studies. The lower portion of the interior wall of Shackleton crater, permanently shadowed from the sun but visible from Earth, is not significantly different in 70-cm scattering properties from diurnally/seasonally sunlit areas of craters with similar morphology.

Acknowledgments

This work was supported in part by grants from the NASA Planetary Geology and Geophysics Program. The authors thank J. Chandler for producing the lunar ephemeris files, J.-L. Margot for assistance in setting up the radar data collection and processing, and the staff of Arecibo and the GBT for observing assistance. The Arecibo Observatory is part of the National Astronomy and Ionosphere Center, which is operated by Cornell University under a cooperative agreement with the National Science Foundation (NSF) and with support from NASA. The Green Bank Telescope is part of the National Radio Astronomy Observatory, a facility of the NSF operated under cooperative agreement by Associated Universities, Inc. B.R. Hawke, D.B.J. Bussey, C.M. Pieters, M.S. Robinson, and an anonymous reviewer provided helpful comments.

References

Black, G.J., Campbell, D.B., Harmon, J.K., 2002. New 70-cm wavelength radar images of Mercury's north polar region. Lunar Planet. Sci. XXXIII. Abstract 1946.

Bussey, D.B.J., Spudis, P.D., Robinson, M.S., 1999. Illumination conditions at the lunar south pole. Geophys. Res. Lett. 26, 1187–1190.

Butler, B.J., Muhleman, D.O., Slade, M.A., 1993. Mercury: Full-disk radar images and the detection and stability of ice at the north pole. J. Geophys. Res. 98, 15003–15024.

Campbell, B.A., Arvidson, R.E., Shepard, M.K., 1993. Radar polarization properties of volcanic and playa surfaces: Applications to terrestrial remote sensing and Venus data interpretation. J. Geophys. Res. 98, 17099–17113.

Campbell, B.A., Campbell, D.B., Chandler, J.F., Hine, A.A., Nolan, M.C., Perillat, P.J., 2003. Radar imaging of the lunar poles. Nature 426, 137–138.

Carrier, W.D., Olhoeft, G.R., Mendell, W., 1991. Physical properties of the lunar surface. In: Heiken, G. (Ed.), Lunar Sourcebook: A User's Guide to the Mean. Cambridge Univ. Press, New York.

Crider, D.H., Vondrak, R.R., 2000. The solar wind as a possible source of lunar polar hydrogen deposits. J. Geophys. Res. 105, 26773–26782.

Eggleton, R.E., Schaber, G.G., 1972. Cayley formation interpreted as basin ejecta. Apollo 16 Prelim. Sci. Report, 29-7–29-16.

Feldman, W.C., and 11 colleagues, 2001. Evidence for water ice near the lunar poles. J. Geophys. Res. 106, 23232–23252.

Ghent, R.R., Leverington, D.W., Campbell, B.A., Hawke, B.R., Campbell, D.B., 2005. Earth-based observations of radar-dark crater haloes on the Moon: Implications for regolith properties. J. Geophys. Res. 110, doi:10.1029/2005JE002425. E09002.

Hapke, B., 1990. Coherent backscatter and the radar characteristics of outer planets satellites. Icarus 88, 407–417.

Harmon, J.K., Slade, M.A., Velez, R.A., Crespo, A., Dryer, M.J., Johuson, J.M., 1994. Radar mapping of Mercury's polar anomalies. Nature 369, 213–215.

Margot, J., Campbell, D.B., Jurgens, R.F., Slade, M.A., 1999. Topography of the lunar poles from radar interferometry: A survey of cold trap locations. Science 284, 1658–1660.

Moore, H.J., Hodges, C.A., Scott, D.H., 1974. Multiringed basins—Illustrated by Orientale and associated features. Proc. Lunar Sci. Conf. V, 71–100.

Nozette, S., Spudis, P.D., Robinson, M.S., Bussey, D.B.J., Lichtenberg, C., Bonner, R., 2001. Integration of lunar polar remote-sensing datasets: Evidence for ice at the lunar south pole. J. Geophys. Res. 106, 23253–23266.

Nozette, S., Lichtenberg, C.L., Spudis, P., Bonner, R., Ort, W., Malaret, E., Robinson, M., Shoemaker, E.M., 1996. The Clementine bistatic radar experiment. Science 274, 1495–1497.

Shorthill, R.W., 1973. Infrared atlas charts of the eclipsed Moon. Moon 7, 22–45.

Simpson, R.A., Tyler, G.L., 1999. Reanalysis of Clementine bistatic radar data from the lunar south pole. J. Geophys. Res. 104, 3845–3862.

Stacy, N.J.S., Campbell, D.B., Ford, P.G., 1997. Radar mapping of the lunar poles: A search for ice deposits. Science 276, 1527–1530.

Thompson, T.W., Roberts, W.J., Hartmann, W.K., Shorthill, R.W., Zisk, S.H., 1979. Blocky craters: Implications about the lunar megaregolith. Moon Planets 21, 319–342.

Wilhelms, D.E., 1987. The Geologic History of the Moon. USGS Prof. Paper 1348.

Wilhelms, D.E., Howard, K.A., Wilshire, H.G., 1979. Geologic map of the south side of the Moon. USGS Map I-1162.